

Anomalous backward scattering of light by a two-side-open subwavelength metallic slit

S. V. Kukhlevsky^a, M. Mechler^b, L. Csapó^c, K. Janssens^d, O. Samek^e

^a*Institute of Physics, University of Pécs, Ifjúság u. 6, Pécs 7624, Hungary*

^b*South-Trans-Danubian Cooperative Research Centre,
University of Pécs, Ifjúság u. 6, Pécs 7624, Hungary*

^c*Institute of Mathematics and Information, University of Pécs, Ifjúság u. 6, Pécs 7624, Hungary*

^d*Department of Chemistry, University of Antwerp, Universiteitsplein 1, B-2610 Antwerp, Belgium*

^e*Institute of Spectrochemistry and Applied Spectroscopy,
Bunsen-Kirchhoff-Str. 11, D-44139 Dortmund, Germany*

The backward scattering of TM-polarized light by a two-side-open subwavelength slit in a metal film is analyzed. We show that the reflection coefficient versus wavelength possesses a Fabry-Perot-like dependence that is similar to the anomalous behavior of transmission reported in the study [Y. Takakura, Phys. Rev. Lett. **86**, 5601 (2001)]. The open slit totally reflects the light at the near-to-resonance wavelengths. In addition, we show that the interference of incident and resonantly backward-scattered light produces in the near-field diffraction zone a spatially localized wave whose intensity is $10 - 10^3$ times greater than the incident wave, but one order of magnitude smaller than the intra-cavity intensity. The amplitude and phase of the resonant wave at the slit entrance and exit are different from that of a Fabry-Perot cavity.

PACS numbers: 78.67Bf; 07.79.Fc; 71.36.+c; 73.20.Mf; 78.66.Bz

I. INTRODUCTION

The most impressive features of light scattering by subwavelength metallic nanostructures are resonant enhancement and localization of the light by excitation of electron waves in the metal (for example, see refs. 1,2,3,4,5,6,7,8,9,10,11,12,13,14,15,16,17,18,19,20,21,22,23,24,25,26,27,28,29,30,31,32,33,34,35,36,37).

In the last few years, a great number of studies have been devoted to the 2D nanostructures in metal films, namely a single slit, a grating of slits and a slit surrounded by parallel grooves. The localization and enhancement of light by a single slit^{1,2,3} can be used in NSOM^{4,5,6,7}. The extraordinary (resonantly enhanced) transmission of light through a grating of slits or a slit surrounded by grooves is expected to find numerous applications in nanophotonics.^{8,9,10} For instance, a nanoslit flanked by a finite array of grooves can act as a lens focusing a light or can produce a μm -size beam that spreads to an angle of only few degrees.^{10,11,12} The quasi-diffraction-free beam optics based on the light transmission through nanoslits was suggested to extend the physical principle of a 2D NSOM to the not-too-distant far-field regime.¹⁴ The high-throughput wavelength selective gratings can be used in photolithography and many kinds of sensors and actuators.^{8,9,10,11,12,13,14,15,16,17,18,19,20,21,22,23,24,25,26,27,28,29,30,31,32,33,34,35,36,37}

Since the paper⁸ of Ebbesen and colleagues on the light anomalous transmission observed for a 2D array of subwavelength apertures in metal films, the phenomenon is intensively discussed in the literature.^{8,9,10,11,12,13,14,15,16,17,18,19,20,21,22,23,24,25,26,27,28,29,30,31,32,33,34,35,36,37}

In the case of a slit array in a thick metal film, the transmission exhibits enhancement due to a pure geometrical reason, the resonant excitation of propagating TM-modes inside the slit waveguide.^{16,18,22} At the resonant wavelengths, the transmitted field increases via the strong coupling of an incident wave with the wave-

guide modes giving a Fabry-Perot-like behavior.^{20,21,36}

In the case of films, whose thickness are too small to support the intra-cavity resonance, the extraordinary transmission can be caused by another mechanism, the generation of resonant surface plasmon polaritons and coupling of them into radiation.^{11,16,22} Both physical mechanisms play important roles in the extraordinary transmission through arrays of two-side-open slits (transmission gratings) and the anomalous reflection by arrays of one-side-open slits (reflection gratings). A model of trapped (waveguide) modes has been recently used to show that an array of two-side-open slits can operate like a reflection grating totally reflecting TE-polarized light.³⁷ The surface plasmons and Rayleigh anomalies were involved in explanation of reflective properties of such kind of a grating.²⁹

The studies^{20,21,23,36} have pointed out that the origin of anomalous scattering of light by a grating of slits (holes) can be better understood by clarifying the transmission and reflection properties of a single subwavelength slit. Along this direction, it was already demonstrated that the intensity of TM-polarized light resonantly transmitting through a single slit can be $10 - 10^3$ times higher than the incident wave^{2,3,36} and that the transmission coefficient versus wavelength possesses a Fabry-Perot-like behavior^{20,36}. Unfortunately, the reflection properties of the slit have received no attention in the literature. The very recent study³⁷ only concerned the problem by regarding the total reflection of TE-polarized light by a grating of two-side-open slits to properties of the independent slit emitters.

In this article, the backward scattering of light by a two-side-open subwavelength slit is analyzed. To compare properties of the light reflection with the extraordinary transmission^{20,36}, we consider the scattering of TM-polarized light by a slit in a thick metallic film of

perfect conductivity. The traditional approach based on the Neerhoff and Mur solutions of Maxwell's equations is used in the computations.^{1,2,3} The article is organized as follows. The theoretical background, numerical analysis and discussion are presented in Section II. The summary and conclusions are given in Section III. The detailed model and method of solution of the Neerhoff and Mur integral equations are presented in the Appendix.

II. NUMERICAL ANALYSIS AND DISCUSSION

It is well known that when a light scattered by a sub-wavelength metallic object, a significant part of the incident light can be scattered backward (reflected) whatever the object be reflecting or transparent. It was recently demonstrated that an array of a two-side-open subwavelength metallic slits effectively reflects light waves at the appropriate resonant conditions.^{29,37} One may suppose that this is true also in the case of a single slit. In this section, we test whether a light wave can be resonantly reflected by a single two-side-open subwavelength metallic slit. To address this question, the energy flux in front of the slit is analyzed numerically under various regimes of the light scattering. In order to compare properties of the light reflection with that of the extraordinary (resonant) transmission^{20,21,36}, we consider the zero-order scattering of a time-harmonic wave of TM-polarized light by a thick slit in a perfectly conducting metal film placed in vacuum. The energy flux \vec{S}_I in front of the slit is compared with the fluxes \vec{S}_{II} and \vec{S}_{III} inside the slit and behind the slit, respectively. The amplitude and phase of the light wave at the slit entrance and exit are compared with that of a Fabry-Perot cavity. The electric \vec{E} and magnetic \vec{H} fields of the light are computed by using the traditional approach based on the Neerhoff and Mur solutions of Maxwell's equations.^{1,2,3} The detailed description of the model and the method of solution of the Neerhoff and Mur integral equations are presented in the Appendix.

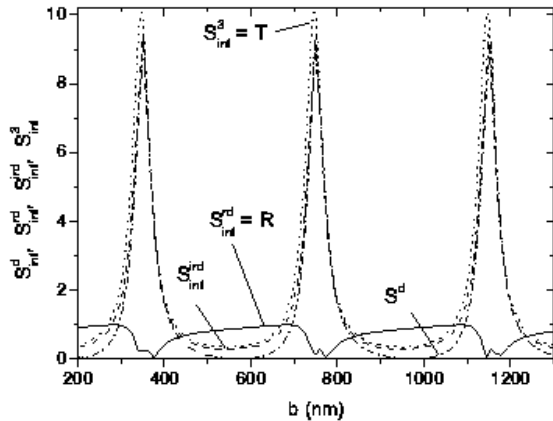
According to the model, the electric $\vec{E}(x, z)$ and magnetic $\vec{H}(x, z)$ fields in front of the slit (region I), inside the slit (region II) and behind the slit (region III) are determined by the scalar fields $U_1(x, z)$, $U_2(x, z)$ and $U_3(x, z)$, respectively. The scalar fields are found by solving the Neerhoff and Mur integral equations. The time averaged Poynting vector (energy flux) \vec{S} of the electromagnetic field is given by $\vec{S} = (c/16\pi)(\vec{E} \times \vec{H}^* + \vec{E}^* \times \vec{H})$. In front of the slit, the field $U_1(x, z) = U^i(x, z) + U^r(x, z) + U^d(x, z)$. The field $U^i(x, z) = \exp(-ikz)$ represents the incident field, which is assumed to be a plane wave of unit amplitude; $U^r(x, z) = U^i(x, 2b - z)$ denotes the field that would be reflected if there were no slit in the film; $U^d(x, z)$ describes the backward diffracted field due to the presence of the slit. The reflection coefficient $R = S_n^{rd}$ is given by the normalized flux $S_n^{rd} = S^{rd}/S^i$ integrated over the slit width $2a$ at the slit entrance ($z = b$), where

S^{rd} is the z component of the backward scattered flux, and S^i is the incident flux along the z direction. The flux $S^{rd} = S^{rd}(U^r, U^d)$ is produced by the interference of the backward scattered fields $U^r(x, z)$ and $U^d(x, z)$. The transmission coefficient $T = S_{int}^3(b)$ is determined by the normalized flux $S_n^3 = S^3/S^i$ integrated over the slit at the slit exit ($z = 0$), where the flux z -component $S^3 = S^3(U^3)$ is produced by the forward scattered (transmitted) field $U^3(x, z)$. In the following analysis, the R reflection and T transmission coefficients are compared with the fluxes S_{int}^d and S_{int}^{ird} obtained by integrating the normalized fluxes $S_n^d = S^d/S^i$ and $S_n^{ird} = S^{ird}/S^i$, respectively.

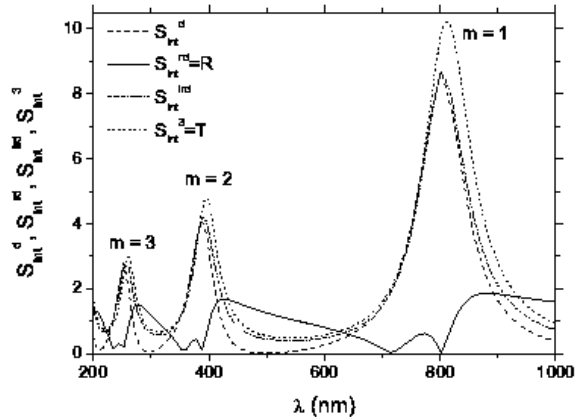
We have analyzed the backward scattering of light for the wide range of scattering conditions determined by values of the wavelength λ , slit width $2a$ and film thickness b . As an example, the reflection coefficient $R = S_{int}^{rd}(b)$ as a function of the film thickness b computed for the wavelength $\lambda = 800$ nm and the slit width $2a = 25$ nm is shown in Fig. 1(a). The transmission coefficient $T = S_{int}^3(b)$ and the integrated fluxes $S_{int}^d(b)$ and $S_{int}^{ird}(b)$ are presented in the figure for the comparison.

We note the reflection resonances of $\lambda/2$ periodicity with the maximums $R_{max} \sim 1$ (total reflection). In agreement with the previous results^{20,21,36}, we see also the transmission resonances having the same period and the peak heights $T \sim \lambda/2\pi a$ at the resonances. It is worth to note the correlation between the positions of maximums and minimums in the reflection and transmission. The resonance positions for the total reflection are somewhat left-shifted with respect to the transmission resonances. The maximums of the transmission coefficient correspond to the reflection minimums. To clarify a role of the fields U^i , U^r , U^d and U^3 in the resonant backward scattering, we compared the integrated flux $S_{int}^{ird}(U^i, U^r, U^d)$ with the fluxes $S_{int}^d(U^d)$ and $S_{int}^3(U^3) = T$. As can be seen from Fig. 1(a), the flux S_{int}^{ird} produced in front of the slit by interference of the incident field $U^i(x, z)$ and backward scattered fields $U^r(x, z)$ and $U^d(x, z)$ is practically undistinguishable from that generated by the backward diffracted field U^d and forward scattered (transmitted) field U^3 . The integrated flux $S_{int}^{ird}(a, b)$ as a function of the slit half-width a and film thickness b is shown in Fig. 1(b). We notice that the widths and shifts of the resonances increase with decreasing the value a . Analysis of Fig. 1(a) indicates that the difference between the integrated fluxes $S_{int}^{rd}(U^r, U^d) = R$ and $S_{int}^3(U^3) = T$ appears due to the interference of the backward diffracted field $U^d(x, z)$ and the reflected field $U^r(x, z)$. Because of the interference, the maximums in transmission are accompanied by the minimums in the reflection.

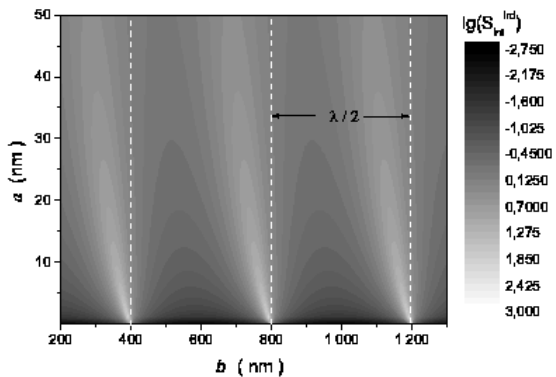
The dispersion of the reflection coefficient $R(\lambda) = S_{int}^{rd}(\lambda)$ for the slit width $2a = 25$ nm and the screen thickness $b = 351$ nm is shown in Fig. 2(a). The integrated fluxes $S_{int}^d(\lambda)$, $S_{int}^{ird}(\lambda)$ and $S_{int}^3(\lambda) = T(\lambda)$ versus the wavelength are shown in the figure for the comparison. We note a very interesting behavior of the dispersion



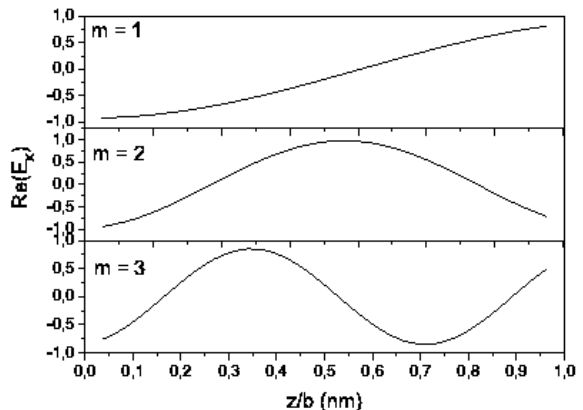
(a)



(a)



(b)



(b)

FIG. 1: (a) The reflection coefficient $R = S_{int}^{rd}(b)$, the transmission coefficient $T = S_{int}^3(b)$, and the integrated fluxes $S_{int}^d(b)$ and $S_{int}^{ird}(b)$ as a function of the film thickness b computed for the wavelength $\lambda = 800$ nm and the slit width $2a = 25$ nm.

(b) The logarithm of the integrated flux $S_{int}^{ird}(a, b)$ as a function of the slit half-width a and film thickness b .

$R(\lambda)$. The coefficient R versus the wavelength λ possesses a Fabry-Perot-like dependence that is similar to the anomalous behavior of transmission $T(\lambda)$ reported in the studies^{20,21,23,36}. In contrast to the sharp transmission peaks, the slit forms very wide reflection bands. At the near-to-resonance wavelengths, the open aperture of the slit totally reflects ($R \sim 1$) the light. In Fig. 2(a), we also note the sharp transmission resonances of $\lambda/2$ periodicity with the maximums at the resonances. In accordance with the studies^{2,3,36}, the height of the first (maximum) peak is given by $T \sim \lambda_R^1/2\pi a$. The val-

FIG. 2: (a) The reflection coefficient $R = S_{int}^{rd}(\lambda)$, the transmission coefficient $T = S_{int}^3(\lambda)$, and the integrated fluxes $S_{int}^d(\lambda)$ and $S_{int}^{ird}(\lambda)$ versus the wavelength λ computed for the slit width $2a = 25$ nm and the screen thickness $b = 351$ nm.

(b) The real part of the normalized electric field x-component $E_x(U_2) = E_x(x, z)$ versus the normalized distance z/b inside the slit cavity at $x = 0$, for the resonant wavelength $\lambda_R^1 = 800$ nm.

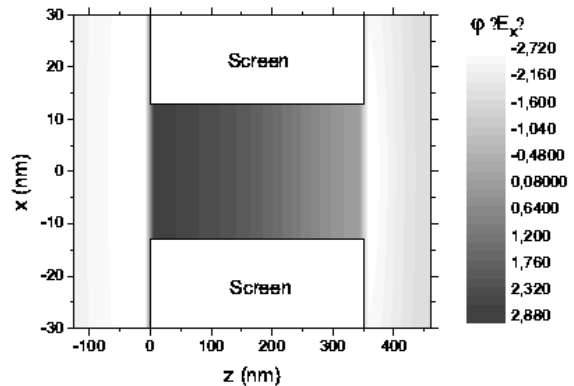
ues of resonance wavelengths λ_R^m ($m = 1, 2, 3, \dots$) are in agreement with the results²⁰. The peak heights, however, are different from the predictions²⁰, but compare well with the results^{2,3,36}. It is worth to note the correlation between the wavelengths for maximums and minimums in the reflection $R(\lambda)$ and transmission $T(\lambda)$. The resonance wavelengths for the total reflection are somewhat red-shifted with respect to the transmission resonances. To understand the physical mechanism of the resonant backward scattering, we also compared the in-

egrated flux $S_{int}^{ird}(U^i, U^r, U^d)$ with the fluxes $S_{int}^d(U^d)$ and $S_{int}^3(U^3) = T$. As can be seen from Fig. 2(a), the integrated fluxes $S_{int}^d(\lambda)$, $S_{int}^{ird}(\lambda)$ and $S_{int}^3(\lambda) = T(\lambda)$ are practically undistinguishable also in the λ -domain (for the b -domain, see Fig. 1(a)). The difference between the integrated fluxes $S_{int}^{rd}(U^r, U^d) = R$ and $S_{int}^3(U^3) = T$ is caused by the interference of the backward diffracted field $U^d(x, z)$ and the reflected field $U^r(x, z)$.

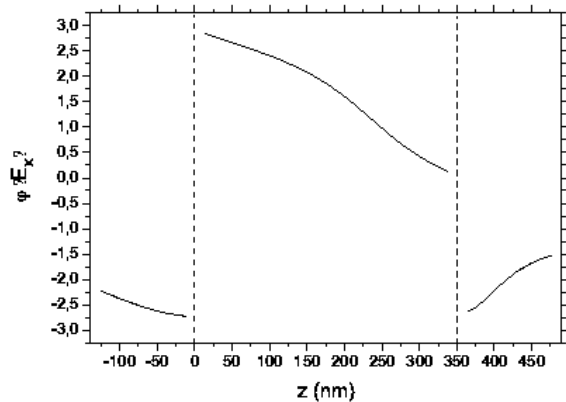
It is not surprising now that the maximums of transmission are accompanied by the minimums of the reflection (Figs. 1(a) and 2(a)). It should be noted in this connection that the behaviors of $R(\lambda)$ and $T(\lambda)$ are similar to that observed in the case²⁹ of excitation of surface plasmons in an array of slit in a thin metal film.

In the study²⁹, the minimums in reflection spectra corresponding to the maximums in the transmission spectra were attributed to the redistribution of the energy of diffracted evanescent order into the propagating order. In the case of a thick film, we explain such a behavior by another physical mechanism, the interference of the backward diffracted field $U^d(x, z)$ and the reflected field $U^r(x, z)$. It can be noted that the total reflection (see, Figs. 1(a) and 2(a)) compare well also with the total reflection effect predicted by the study³⁷ for TE-polarized light scattered by a grating of two-side-open slits in a thick metal film. However, the dispersions $R(\lambda)$ and $T(\lambda)$ are in contrast to the relation $R(\lambda) + T(\lambda) = 1$ and the positions of reflection minimums and transmission maximums derived in the study³⁷. The difference can be perhaps attributed to the boundary conditions used in the study³⁷ for the TE polarization. Indeed, in our model we consider the incident wave with TM polarization. According to the theory of waveguides, the vectorial wave equations for this polarization can be reduced to one scalar equation describing the magnetic field H of TM modes. The electric component E of these modes is found using the field H and Maxwell's equations. The TM scalar equation for the component H is decoupled from the similar scalar equation describing the field E of TE (transverse electric) modes. Hence, the formalism works analogously for TE polarization exchanging the E and H fields. The symmetry, however, is broken by using the different boundary conditions for the TM and TE polarizations.

The dispersions $S_{int}^d(\lambda)$, $S_{int}^{ird}(\lambda)$ and $S_{int}^3(\lambda) = T(\lambda)$ shown in Fig. 2(a) indicate the wave-cavity interaction behavior, which is similar to that in the case of a Fabry-Perot resonator. The fluxes $S_{int}^d(U^d)$, $S_{int}^{ird}(U^i, U^r, U^d)$ and $S_{int}^3(U^3) = T$ exhibit the Fabry-Perot-like maximums around the resonance wavelengths $\lambda_R^m \sim 2b/m$. It can be mentioned that the small shifts of resonant wavelengths in the transmission spectra from the values $2b/m$ are explained in the studies^{20,21,36}. In order to understand the connection between the Fabry-Perot-like resonances and the total reflection, we computed the amplitude and phase of the light wave at the resonant and near-resonant wavelengths inside and outside the slit cavity (see, Figs. 2(b), 3 and 4). At the resonance wave-



(a)



(b)

FIG. 3: (a) The phase distribution $\varphi(x, z)$ of the electric field x -component $E_x(x, z)$ inside and outside the slit. The field component $E_x(x, z)$ is given by $E_x(U^i, U^r, U^d)$, $E_x(U^2)$ and $E_x(U^3)$ in the regions I, II and III, respectively.

(b) The phase distribution $\varphi(x, z)$ at $x = 0$. The slit width $2a = 25$ nm, the film thickness $b = 351$ nm and the wavelength $\lambda = 800$ nm.

lengths, the intra-slit fields possess maximum amplitudes with Fabry-Perot-like spatial distributions (Fig. 2(b)). However, in contrast to the Fabry-Perot-like modal distributions, the resonant configurations are characterized by antinodes of the electric field at each open aperture of the slit. Such a behavior is in agreement with the results¹⁸. It is interesting that at the slit entrance and exit, the amplitudes E_x of the resonant field configurations possess the Fabry-Perot-like phase shifts on the values of π and 2π , respectively (Fig. 3). The integrated fluxes $S_{int}^{ird}(U^i, U^r, U^d)$, $S_{int}^d(U^d)$ and $S_{int}^3(U^3)$, at the first resonant wavelength λ_R^1 , exhibit enhancement by

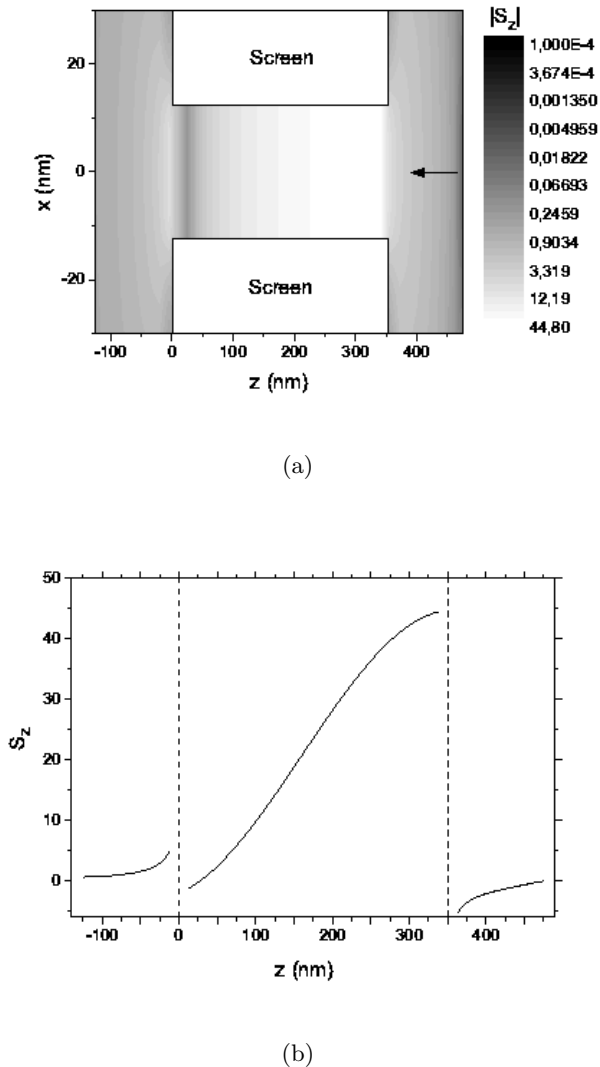


FIG. 4: (a) The spatial distribution $|S_z(x, z)|$ of the absolute value of the normalized energy flux along the z direction inside and outside the slit. The distribution $|S_z(x, z)|$ is shown in the logarithmical scale. The flux S_z is given by the normalized fluxes $S^{ird}(U^i, U^r, U^d)/S^i(U^i)$, $S^2(U^2)/S^i(U^i)$ and $S^3(U^3)/S^i(U^i)$ for the regions I, II and III, respectively.

(b) The energy flux distribution $S_z(x, z)$ at $x = 0$. The slit width $2a = 25$ nm, the film thickness $b = 351$ nm and the wavelength $\lambda = 800$ nm.

a factor $\lambda/2\pi a \sim 10$ with respect to the incident wave (Fig. 2(a)). For the comparison, the normalized resonant fluxes $S_n^{ird}(U^i, U^r, U^d)$ and $S_n^3(U^3)$ in the near-field zone ($z \sim -2a$) are about 5 times greater than the incident wave (see, Fig. 4). It should be stressed that the resonantly enhanced intra-cavity intensity $S_n^2(U^2)$ is about 10 times higher than the resonant fluxes $S_n^{ird}(U^i, U^r, U^d)$ and $S_n^3(U^3)$ localized in the near field zone in front of the slit and behind the slit, respectively (Fig. 4). The

interference of the incident $U^i(x, z)$ wave and the backward scattered fields $U^r(x, z)$ and $U^d(x, z)$, at the resonant wavelengths $\lambda_R^m \sim 2b/m$, produces in the near-field diffraction zone a strongly localized wave whose normalized flux $S_n^{ird}(U^i, U^r, U^d)$ is $\lambda/2\pi a \sim 10 - 10^3$ times greater than the incident wave, but about one order of magnitude smaller than the resonant intra-cavity intensity. It is clear now that the physical mechanism responsible for the total reflection ($S_{int}^{rd} \sim 1$) is the interplay of the backward diffracted field $U^d(x, z)$ and the reflected field $U^r(x, z)$ in the energy flux $\vec{S} \sim (\vec{E} \times \vec{H}^* + \vec{E}^* \times \vec{H})$, at the near-to-resonance wavelengths.

III. SUMMARY AND CONCLUSION

In the present paper, the backward scattering of TM-polarized light by a two-side-open subwavelength slit in a metal film has been analyzed. We predict that the reflection coefficient versus wavelength possesses a Fabry-Perot-like dependence that is similar to the anomalous behavior of transmission. The open slit totally reflects the light at the near-to-resonance wavelengths. The resonance wavelengths for the total reflection are somewhat red-shifted with respect to the transmission resonances. The sharp resonant maximums of transmission are accompanied by the wide minimums of the reflection. In addition, we showed that the interference of incident and resonantly backward-scattered light produces in the near-field diffraction zone a strongly localized wave whose intensity is greater than the incident wave by a factor $\lambda/2\pi a \sim 10 - 10^3$ and about one order of magnitude smaller than the intra-cavity intensity. The correlation between the amplitude and phase distributions of light waves inside and outside the slit was also investigated. The slit cavity was compared with a Fabry-Perot resonator. We showed that the amplitude and phase of the resonant wave at the slit entrance and exit are different from that of a Fabry-Perot cavity. The physical mechanism responsible for the total reflection is the interplay of the backward diffracted field $U^d(x, z)$ and the reflected field $U^r(x, z)$ in the energy flux $\vec{S} \sim (\vec{E} \times \vec{H}^* + \vec{E}^* \times \vec{H})$ at the near-to-resonance wavelengths. The wavelength-selective total reflection of light by two-side-open metal slits may find application in many kinds of sensors and actuators. The $(10 - 10^3)$ -times and $(10^2 - 10^5)$ -times enhancement of the light intensity in front of the slit and inside the slit can be used in reflective nanooptics and in intra-cavity spectroscopy of single atoms. We believe that the presented results gains insight into the physics of resonant scattering of light by subwavelength nano-slits in metal films.

Acknowledgments

This study was supported by the Fifth Framework of the European Commission (Financial support from the

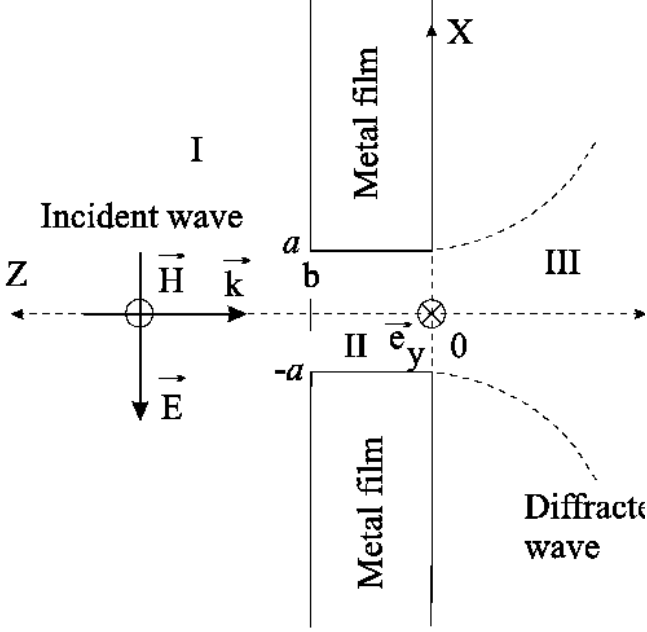


FIG. 5: Propagation of a continuous wave through a subwavelength nano-sized slit in a thick metal film.

EC for shared-cost RTD actions: research and technological development projects, demonstration projects and combined projects. Contract NG6RD-CT-2001-00602). The authors thank the Computing Services Centre, Faculty of Science, University of Pécs, for providing computational resources.

Appendix

We briefly summarize the Neerhoff and Mur formulation^{1,3} describing the near-field diffraction of a plane continuous wave by a subwavelength slit of width $2a$ in a perfectly conducting metal screen of thickness b .

The slit is illuminated by a normally incident plane wave under TM polarization (magnetic-field vector parallel to the slit), as shown in Fig. 5. The magnetic field of the wave is assumed to be time harmonic and constant in the y direction:

$$\vec{H}(x, y, z, t) = U(x, z)\exp(-i\omega t)\vec{e}_y. \quad (1)$$

The electric field of the wave is found from the scalar field $U(x, z)$ using Maxwell's equations. The restrictions in Eq. 1 reduce the diffraction problem to one involving a single scalar field $U(x, z)$ in two dimensions. The field is represented by $U_j(x, z)$ ($j=1,2,3$ in region I, II and III, respectively), and satisfies the Helmholtz equation: $(\nabla^2 + k_j^2)U_j = 0$, where $j = 1, 2, 3$. In region I, the field

$U_1(x, z)$ is decomposed into three components:

$$U_1(x, z) = U^i(x, z) + U^r(x, z) + U^d(x, z), \quad (2)$$

each of which satisfies the Helmholtz equation. U^i represents the incident field:

$$U^i(x, z) = \exp(-ik_1 z). \quad (3)$$

U^r denotes the reflected field without a slit:

$$U^r(x, z) = U^i(x, 2b - z). \quad (4)$$

Finally, U^d describes the diffracted field in region I due to the presence of the slit. With the above set of equations and standard boundary conditions for a perfectly conducting screen, a unique solution exists for the diffraction problem. To find the field, the 2-dimensional Green's theorem is applied with one function given by $U(x, z)$ and the other by a conventional Green's function:

$$(\nabla^2 + k_j^2)G_j = -\delta(x - x', z - z'), \quad (5)$$

where (x, z) refers to a field point of interest; x', z' are integration variables, $j = 1, 2, 3$. Since U_j satisfies the Helmholtz equation, Green's theorem reduces to

$$U(x, z) = \int_{Boundary} (G\partial_n U - U\partial_n G)dS. \quad (6)$$

The unknown fields $U^d(x, z)$ (for $b < z < \infty$), $U_3(x, z)$ (for $-\infty < z < 0$) and $U_2(x, z)$ (for $|x| < a$ and $0 < z < b$) are found using the reduced Green's theorem and boundary conditions on G . The boundary fields are defined by

$$U_0(x) = U_2(x, z)|_{z \rightarrow 0+}, \quad (7)$$

$$DU_0(x) = \partial_z U_2(x, z)|_{z \rightarrow 0+}, \quad (8)$$

$$U_b(x) = U_2(x, z)|_{z \rightarrow b-}, \quad (9)$$

$$DU_b(x) = \partial_z U_2(x, z)|_{z \rightarrow b-}. \quad (10)$$

In regions I and III the two Green's functions are given by

$$G_1(x, z; x', z') = \frac{i}{4}[H_0^{(1)}(k_1 R) + H_0^{(1)}(k_1 R')], \quad (11)$$

$$G_3(x, z; x', z') = \frac{i}{4}[H_0^{(1)}(k_3 R) + H_0^{(1)}(k_3 R')], \quad (12)$$

where $H_0^{(1)}$ is the Hankel function, and

$$R = \sqrt{(x - x')^2 + (z - z')^2}, \quad (13)$$

$$R' = \sqrt{(x - x')^2 + (z + z' - 2b)^2}, \quad (14)$$

$$R'' = \sqrt{(x - x')^2 + (z + z')^2}. \quad (15)$$

In region II, the Green's function is given by

$$G_2(x, z; x', z') = \frac{i}{4a\gamma_0}\exp(i\gamma_0|z - z'|) + \frac{i}{2a}\sum_{m=1}^{\infty}\gamma_m^{-1} \\ \times \cos[m\pi(x + a)/2a]\cos[m\pi(x' + a)/2a] \\ \times \exp(i\gamma_m|z - z'|), \quad (16)$$

where $\gamma_m = [k_2^2 - (m\pi/2a)^2]^{1/2}$. The field can be found at any point once the four unknown functions in Eqs. 7-10 have been determined. The functions are completely determined by a set of the four integral equations:

$$2U_b^i(x) - U_b(x) = \frac{\epsilon_1}{\epsilon_2} \int_{-a}^a G_1(x, b; x', b) DU_b(x') dx' \quad (17)$$

$$U_0(x) = \frac{\epsilon_3}{\epsilon_2} \int_{-a}^a G_3(x, 0; x', 0) DU_0(x') dx' \quad (18)$$

$$\begin{aligned} \frac{1}{2}U_b(x) = & - \int_{-a}^a [G_2(x, b; x', 0) DU_0(x') \\ & - U_0(x') \partial_{z'} G_2(x, b; x', z')|_{z \rightarrow 0^+}] dx' \\ & + \int_{-a}^a [G_2(x, b; x', b) DU_b(x')] dx' \quad (19) \end{aligned}$$

$$\begin{aligned} \frac{1}{2}U_0(x) = & - \int_{-a}^a [G_2(x, 0; x', b) DU_b(x') \\ & - U_b(x') \partial_{z'} G_2(x, 0; x', z')|_{z \rightarrow b^-}] dx' \\ & - \int_{-a}^a [G_2(x, 0; x', 0) DU_0(x')] dx' \quad (20) \end{aligned}$$

where $|x| < a$, and $U_b^i(x) = \exp(-ik_1b)$. The coupled integral equations 17-20 for the four boundary functions are solved numerically. The magnetic $\vec{H}(x, z, t)$ and electric $\vec{E}(x, z, t)$ fields of the diffracted wave in region III are

found by using the reduced Green's theorem for $U_3(x, z)$. The fields are given by

$$\vec{H}(x, z) = i\epsilon_3 \sum_{j=1}^N C_j^0(x, z) \vec{e}_y, \quad (21)$$

$$E_x(x, z) = -\sqrt{\epsilon_3} \sum_{j=1}^N \frac{z}{\sqrt{(x-x_j)^2 + z^2}} C_j^1(x, z), \quad (22)$$

$$E_y(x, z) = 0, \quad (23)$$

$$E_z(x, z) = \sqrt{\epsilon_3} \sum_{j=1}^N \frac{x-x_j}{\sqrt{(x-x_j)^2 + z^2}} C_j^1(x, z), \quad (24)$$

where

$$C_j^i(x, z) = \frac{a}{N\epsilon_2} (D\vec{U}_0)_j H_i^{(1)} \left[k_3 \sqrt{(x-x_j)^2 + z^2} \right] \quad (25)$$

and $x_j = 2a(j-1/2)/N - a$, $j = 1, 2, \dots, N$; $N > 2a/z$; $H_1^{(1)}$ is the Hankel function. The coefficients $(D\vec{U}_0)_j$ are found by solving numerically the four integral equations 17-20. For more details of the model and the numerical solution of the coupled integral equations 17-20 see refs.^{1,3}.

-
- ¹ F. L. Neerhoff, G. Mur G, Appl. Sci. Res. **28**, 73 (1973).
² R.F. Harrington, D.T. Auckland, IEEE Trans. Antennas Propag **AP28**, 616 (1980).
³ E. Betzig, A. Harootunian, A. Lewis, M. Isaacson, Appl. Opt. **25**, 1890 (1986).
⁴ E.A. Ash, G. Nicholls, Nature (London) **237**, 510 (1972).
⁵ A. Lewis, K. Lieberman, Nature (London) **354**, 214 (1991).
⁶ E. Betzig, J.K. Trautman, T.D. Harris, J.S. Weiner, R.L. Kostelak, Science **251**, 1468 (1991).
⁷ D.W. Pohl, D. Courjon, Eds., *Near Field Optics*, NATO ASI Series E Vol. 242 (The Netherlands, Dordrecht: Kluwer, 1993).
⁸ T.W. Ebbesen, H.J. Lezec, H.F. Ghaemi, T. Thio, P.A. Wolff, Nature (London) **391**, 667 (1998).
⁹ J.R. Sambles, Nature (London) **391**, 641 (1998).
¹⁰ H.J. Lezec, A. Degiron, E. Devaux, R.A. Linke, Martin-Moreno, F.J. Garcia-Vidal, T.W. Ebbesen, Science **297**, 820 (2002).
¹¹ F.J. Garcia-Vidal, H.J. Lezec, T.W. Ebbesen, L. Martin-Moreno, Phys. Rev. Lett. **90**, 231901 (2003).
¹² F.J. Garcia-Vidal, L. Martin-Moreno, H.J. Lezec, T.W. Ebbesen, Appl. Phys. Lett. **83**, 4500 (2003).
¹³ A. Dogariu, M. Hsu, L.J. Wang, Opt. Comm. **220**, 223 (2003).
¹⁴ S.V. Kukhlevsky, M. Mechler, Opt. Comm. **231**, 35 (2004).
¹⁵ U. Schroter, D. Heitmann, Phys. Rev. B **58**, 15419 (1998).
¹⁶ J. A. Porto, F.J. Garcia-Vidal, J.B. Pendry, Phys. Rev. Lett. **83**, 2845 (1999).
¹⁷ M.M.J. Treacy, Phys. Rev. Lett. **75**, 606 (1999).
¹⁸ S. Astilean, Ph. Lalanne, M. Palamaru, Opt. Commun. **175**, 265 (2000).
¹⁹ L. Salomon, F.D. Grillot, A.V. Zayats, F. de Fornel, Phys. Rev. Lett. **86**, 1110 (2001).
²⁰ Y. Takakura, Phys. Rev. Lett. **86**, 5601 (2001).
²¹ F.Z. Yang, J.R. Sambles, Phys. Rev. Lett. **89**, 063901 (2002).
²² A.P. Hibbins, J.R. Sambles, C.R. Lawrence, Appl. Phys. Lett. **81**, 4661 (2002).
²³ F.J. Garcia-Vidal, L. Martin-Moreno, Phys. Rev. B **66**, 155412 (2002).
²⁴ Q. Cao, P. Lalanne, Phys. Rev. Lett. **88**, 057403 (2002).
²⁵ I.I. Smolyaninov, A.V. Zayats, A. Stanishevsky, C.C. Davis, Phys. Rev. B **66**, 205414 (2002).
²⁶ A. Barbara, P. Quemerais, E. Bustaret, T. Lopez-Rios, Phys. Rev. B **66**, 161403 (2002).
²⁷ E. Altewischer, M.P. van Exter, J.P. Woerdman, Nature (London) **418**, 304 (2002).
²⁸ A.M. Dykhne, A.K. Sarychev, V.M. Shalaev, Phys. Rev. B **67**, 195402 (2003).
²⁹ J.M. Steele, C.E. Moran, A. Lee, C.M. Aguirre, N.J. Halas, Phys. Rev. B **68**, 205103 (2003).
³⁰ A. Naweed, F. Baumann, W.A. Bailey, A.S. Karakashian, W.D. Goodhue, J. Opt. Soc. Am. B **20**, 2534 (2003).
³¹ Z.J. Sun, Y.S. Jung, H.K. Kim, Appl. Phys. Lett. **83**, 3021 (2003).
³² X.L. Shi, L. Hesselink, R.L. Thornton, Opt. Lett. **28**, 1320 (2003).
³³ H.F. Schouten, T.D. Visser, D. Lenstra, H. Blok, Phys. Rev. E **67**, 036608 (2003).
³⁴ A. Nahata, R.A. Linke, T. Ishi, K. Ohashi, Opt. Lett. **28**,

- 423 (2003).
- ³⁵ G. Gomez-Santos, Phys. Rev. Lett. **90**, 077401 (2003).
- ³⁶ S.V. Kukhlevsky, M. Mechler, L. Csapo, K. Janssens, O. Samek, Phys. Rev. B **70**, 195428 (2004).
- ³⁷ A.G. Borisov, F.G. Garcia de Abajo, S.V. Shabanov, Phys. Rev. B **71**, 075408 (2005).
- ³⁸ K.R. Li, M.I. Stockman, D.J. Bergman, Phys. Rev. Lett. **91**, 227402 (2003).
- ³⁹ M. Labardi, M. Zavelani-Rossi, D. Polli, G. Cerullo, M. Allegrini, S. De Silvestri, O. Svelto, Appl. Phys. Lett. **86**,031105 (2005).
- ⁴⁰ Y. BEN-ARYEH, International J. Quantum Information **3**,111 (2005).